

Metal-insulator transition in copper oxides induced by apex displacements

Swagata Acharya,¹ Cédric Weber,¹ Evgeny Plekhanov,¹ Dimitar Pashov,¹ A Taraphder,² and Mark Van Schilfgaarde¹

¹King's College London, Theory and Simulation of Condensed Matter, The Strand, WC2R 2LS London, UK*

²Department of Physics and Centre for Theoretical Studies,
Indian Institute of Technology Kharagpur, India 721302

High temperature superconductivity has been found in many kinds of compounds built from planes of Cu and O, separated by spacer layers. Understanding why critical temperatures are so high has been the subject of numerous investigations and extensive controversy. To realize high temperature superconductivity, parent compounds are either hole-doped, such as La_2CuO_4 (LCO) with Sr (LSCO), or electron doped, such as Nd_2CuO_4 (NCO) with Ce (NCCO). In the electron doped cuprates, the antiferromagnetic phase is much more robust than the superconducting phase. However, it was recently found that the reduction of residual out-of-plane apical oxygens dramatically affects the phase diagram, driving those compounds to a superconducting phase. Here we use a recently developed first principles method to explore how displacement of the apical oxygen (A-O) in LCO affects the optical gap, spin and charge susceptibilities, and superconducting order parameter. By combining quasi-particle self-consistent GW (QSGW) and dynamical mean field theory (DMFT), that LCO is a Mott insulator; but small displacements of the apical oxygens drive the compound to a metallic state through a localization/delocalization transition, with a concomitant maximum d -wave order parameter at the transition. We address the question whether NCO can be seen as the limit of LCO with large apical displacements, and elucidate the deep physical reasons why the behaviour of NCO is so different than the hole doped materials. We shed new light on the recent correlation observed between T_c and the charge transfer gap, while also providing a guide towards the design of optimized high- T_c superconductors. Further our results suggest that strong correlation, enough to induce Mott gap, may not be a prerequisite for high- T_c superconductivity.

Since their discovery, the electronic structure of the high temperature superconductors has been a subject of intensive theoretical attention as well as controversy, a situation that continues even today. A landmark question to understand these materials is how their physical properties follow from their electronic and structural properties, and how key parameters govern the maximum critical temperature T_c^{max} . Relating T_c^{max} to a single variable has eluded physicists so far, because the

observed correlation between T_c^{max} and structural properties across materials involves many kinds of them. In this work we propose a theoretical experiment, where we study the electronic modifications induced by displacements of the apical oxygen (A-O), in a typical copper oxide with the T perovskite structure. Recently, two main mechanisms have been put forward to explain the variation in T_c^{max} : i) on one hand, one body terms involving out-of-plane molecular orbitals (axial orbitals with circular symmetry in the basal plane involving a mixture of Cu $4s$, Cu $3d_{z^2-3r^2}$, apical-oxygen $2p_z$) [6] ii) many body effects stemming from the in-plane Mott physics [5, 7] either in one or three band models. In this work, we examine this picture carefully by using a state-of-the-art approach, which treats both the many body effects and one-electron terms on the same footing. We study the parent compounds La_2CuO_4 (LCO) of prototypical hole doped compounds $\text{La}_{2-x}\text{Sr}_x\text{CuO}_4$. We use a realistic theoretical approach, namely the quasi-particle self-consistent GW theory combined with dynamical mean field theory [8, 9] (QSGW+DMFT), as implemented in the Questaal package[10] for QSGW, and Haule's implementation of DMFT [11] (see method section hereafter). GW and DMFT taken together allows for a better treatment of both non-local and local fluctuations. The parent pristine cuprate compound has for decades been known for its complexities in both local and non-local fluctuations. As we show, when the A-O are displaced from their equilibrium position, the role of non-local fluctuations in spin, charge and orbital sectors is non-trivially modified. The present scheme allows us to address many of these entangled issues in both single and two-particle sectors. We carefully analyze how single particle states, the bare charge transfer energy, the correlated spectral functions, and the optics evolve with displacement of the A-O from its equilibrium position, without distorting the otherwise octahedral geometry and the crystal symmetry. We represent the displacement of the A-O along the c axis by δ , such that the (Cu,A-O) bond length expands or increases from its pristine geometry for $\delta>0$, and contracts for $\delta<0$. We evaluate the local irreducible vertex to construct the dynamical spin and charge susceptibilities, respectively $\chi_s(Q, \Omega)$ and $\chi_c(Q, \Omega)$ [12].

Fig. 1a shows the charge gap extracted from the spectral functions of LCO upon displacement δ . Firstly, we find that pristine LCO is a paramagnetic Mott insulator, with a charge gap of ≈ 0.7 eV. The imaginary part of the Cu $d_{x^2-y^2}$ self energy $\Sigma_d(i\omega)$ (see Fig. 1c) is singular

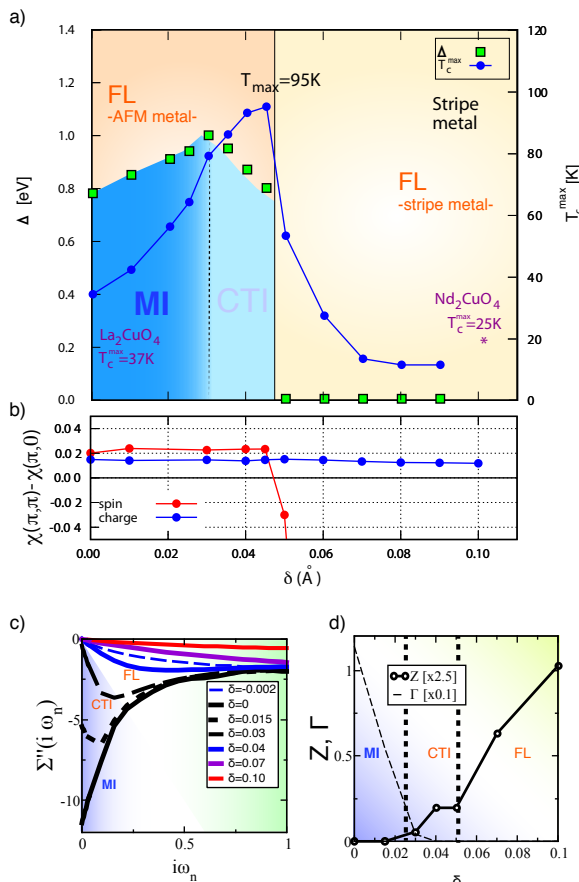


FIG. 1. **Phase diagram:** (Colors online) a) Charge gap Δ (squares, left ordinates) with respect to δ , the apical oxygen displacement. We show also the estimated critical temperature at optimal doping T_c^{\max} (circles, right ordinates). We find that optimum critical temperature is largest at the insulator to metal transition ($\delta = 0.045$). b) Relative static susceptibilities $\chi(\pi, \pi) - \chi(\pi, 0)$ for spin (blue circles) and charge (red circles) degrees of freedom. c) Imaginary part of the Cu $d_{x^2-y^2}$ self-energy $\Sigma''(i\omega)$ on the Matsubara axis for pristine LCO (bold line) and distorted LCO. For $\omega < 0.03$, the self energy is extrapolated with a polynomial fit to $\omega = 0$. The large scattering rate and the pole in the self energy for $\delta < 0.02$ indicate a Mott insulating phase (MI), whereas for $\delta > 0.03$ we obtain a charge transfer insulator with non-quadratic self-energies (CTI). d) Imaginary part of the self energy extrapolated to zero frequency $\Gamma = -\Sigma''(i\omega \rightarrow 0)$ and quasi-particle weight Z .

with a large degree of incoherence.

For small, positive δ ($< 0.03\text{\AA}$), the system remains a Mott insulator (MI) and we observe a direct correlation of the charge gap with the Cu-AO distance. This can be explained by the reduction of the scattering rate (see Fig. 1c), which in turn reduces the incoherence and spread of the spectral weight features in the lower and upper Hubbard bands. This is also supported by the band structure provided in the supplementary material SI (see Fig.1 of the SI).

For $\delta > 0.03\text{\AA}$, the self energy remains non quadratic, but with a finite (albeit small) quasi-particle weight Z (see Fig. 1d)). The incoherence is mostly lost and we obtain hence a crossover from a MI to a charge transfer insulator (CTI). At critical displacement $\delta_c = 0.045$ the gap collapses and we obtain a correlated metal for $\delta > 0.045\text{\AA}$ (Fermi liquid).

We now turn to the discussion of the superconducting order parameter (see Fig. 1a). We estimate the d-wave superconducting pairing correlator following the method outlined in Ref. [13]. We use the magnitude of the static d-wave order parameter as a proxy for the maximum superconducting temperature at optimal doping (T_c^{\max}) [7]. Remarkably, we find that T_c^{\max} [7] is largest at the localization/delocalization transition. This was already obtained in model Hamiltonian studies [14]. We confirm this model Hamiltonian prediction in a realistic framework: the apex displacement provides more than a gedanken experiment, it provides a realization of the Mott transition in a given material with a nearly *ab initio* hamiltonian, by varying a single control parameter. Our analysis indicates that the phase transition at δ_c shapes not only the normal-state phase diagram, but strikingly leaves its mark on the complex structure of the superconducting condensate that is born out of this unusual normal state. It provides hence a guide towards the design of optimized superconductors.

Furthermore, an anti-linear correlation between T_c^{\max} and the charge gap has been suggested both on theoretical [7] and experimental grounds [5]. We note that a similar trend is obtained in our data for the CTI phase: the charge gap is reduced as the apex distance is shifted by more than $\delta = 0.03\text{\AA}$, but the critical temperature T_c^{\max} increases up to the maximum of $\sim 100\text{ K}$ at δ_c . This is understood in the picture of a loss of correlation strength, which in turn increases T_c^{\max} in the vicinity of the delocalization transition, a many body origin.

Interestingly, for small but positive δ ($< 0.03\text{\AA}$) the increase of T_c^{\max} correlates with the Cu-AO distance. This matches with the early prediction of O. K Andersen and collaborators [6]. They concluded that T_c^{\max} is controlled by the energy of the axial orbital, a hybrid between Cu 4s, A-O 2p_z, and Cu 3d orbitals. Our results provide a similar trend with the Cu-AO distance for $\delta < 0.03$. Indeed, for pristine LCO and for small displacements ($\delta < 0.03\text{\AA}$), the QSGW band structure indicates that the lower Hubbard d band of pristine LCO, a hybrid between Cu- $d_{x^2-y^2}$ and in-plane oxygens, also has $\approx 10\%$ of axial character (see Fig. 1a and the table of the supplementary materials). The formation of the axial orbital stems from one-body part of the Hamiltonian and it is present in both DFT and GW, however, the non-local fluctuations in GW suppress the axial orbital contribution at the Fermi level significantly.

Finally, we note that the phase diagram is extremely asymmetric in δ . We obtain insulating DMFT solutions

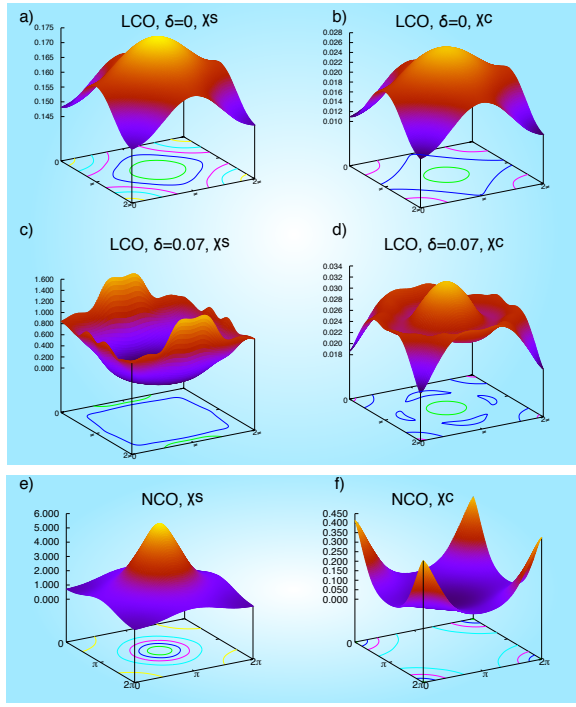


FIG. 2. **Spin and charge fluctuations:** Static spin fluctuations $X^s(k, \omega = 0)$ for a) pristine LCO, c) distorted LCO ($\delta = 0.07$) and e) NCO. Static charge fluctuations $X^c(k, \omega = 0)$ for b) pristine LCO, d) distorted LCO ($\delta = 0.07$) and f) NCO.

for compressions of the AO up to $\delta = -0.05$ and the charge gap increases monotonically for all such displacements. This is explained by an increased charge-transfer energy scale for Cu- $d_{x^2-y^2}$ and O- $p_{x,y}$.

Remarkably, at the critical displacement δ_c , we observe a concomitant change of momentum in the spin fluctuations associated with the gap collapse. We show in Fig. 2a the momentum resolved static magnetic susceptibility for pristine LCO. The susceptibility is peaked at $\mathbf{Q} = (\pi, \pi)$, but with a broad width, denoting short-range antiferromagnetic super-exchange J in direct space. For displacements larger than δ_c , we observe a clear shift of the peak to $\mathbf{Q} = (\pi, 0)$ (Fig. 2c).

The relative static susceptibilities $\chi(\pi, \pi) - \chi(\pi, 0)$ provide an order parameter to track the change of magnetic pitch vector (see Fig. 1b). While the spin fluctuations are located at $\mathbf{Q} = (\pi, \pi)$ for pristine LCO and $\delta < \delta_c$, they abruptly evolve to $\mathbf{Q} = (\pi, 0)$ after the transition (see Fig. 1b).

This is reminiscent of finite asymmetry present in the orthorhombic structure of pristine LCO [15]. Since the orthorhombic phase does not respect the $x-y$ rotational invariance, the peak is larger at $(0, \pi)$ than $(\pi, 0)$. As the incoherence is lost, and the quasi-particle weight increases, the spectral features near the gap edge recover

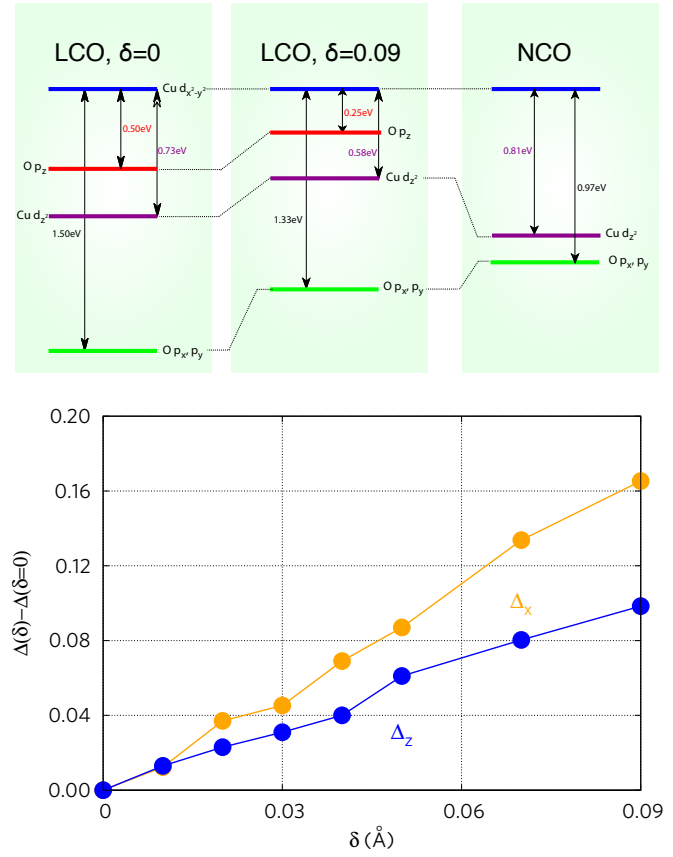


FIG. 3. **Energy levels and charge transfer energy:** (Colors online) The relative positions of the relevant QSGW orbitals for $\delta = 0, 0.09$ and NCO (upper panel). Variation upon apex displacement of the in-plane charge transfer energy $\Delta_x = \epsilon_{p_x} - \epsilon_{d_{x^2-y^2}}$ and of the out-of-plane Cu-AO charge transfer energy $\Delta_z = \epsilon_{p_z} - \epsilon_{d_{z^2-r^2}}$ (lower panel).

the small structural asymmetry (for small Z the spectral feature in the lower band are flat), and in turn provides a magnetic transition from antiferromagnetic to a striped metallic phase. Interestingly, the charge fluctuations remain peaked for LCO at all time at $\mathbf{Q} = (\pi, \pi)$ (see Fig. 2b,d), and they remain small in amplitude throughout the transition.

Under compression ($\delta < 0$), the spin susceptibility peak survives at $\mathbf{Q} = (\pi, \pi)$, suggesting that there is no significant change in the nesting and AFM fluctuations.

Once the AO is pushed far from Cu ($\delta > 0$), however, a localization/delocalization transition with a concomitant magnetic transition from AFM to a stripe phase, originates from the change in the shape and strength of the spin susceptibility. The latter drives charge fluctuations, which reduce the local moment and the gap.

The pioneering work of Zaanen Sawatzky Allen [16] and their sharp (so called ZSA) boundary between charge transfer metals and charge transfer insulators is the canonical picture to describe the copper oxides. The vari-

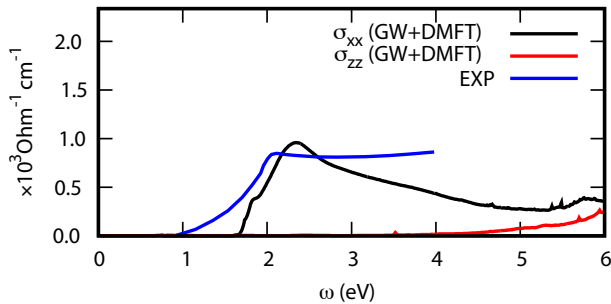


FIG. 4. **Optics:** Theoretical optical conductivity $\sigma(\omega)$ obtained with the QSGW+DMFT approach for the in-plane (σ_{xx}) and out-of-plane components (σ_{zz}). We emphasize that these results are a prediction from an essentially *ab initio* hamiltonian. We obtain remarkable agreement with experimental data, reproduced from Ref. [17], which validates the theoretical approach.

ation of the charge transfer gap (see Fig. 1a) suggests naively that the charge transfer energy between the in-plane Cu 3d and the in-plane oxygens is affected, as it is believed to determine the strength of correlations in a charge transfer system.

It would be expected that the Cu-AO distance would directly affect the in-plane charge transfer energy: the negatively charged apical oxygen increases the electrostatic potential at the copper site, and as it is removed we expect a decrease of the charge transfer energy $\Delta_x = \epsilon_{p_x} - \epsilon_{d_{x^2-y^2}}$.

However, our calculations show that the electrostatic energy changes only by 0.2 eV across the transition (see Fig. 3). This effect is, however, sufficient to drive the compound to a metal, and hence confirms that LCO is sitting at the boundary between a metal and insulator.

We also find that the out-of-plane Cu-AO charge transfer is changing on an energy scale of ≈ 0.1 eV (see Fig. 3). The latter stems from the re-hybridization between the Cu 3d and out of plane orbitals, as surmised by O. Andersen and coworkers [6], via non-local correlations effects captured by the GW. Indeed, we observe that the band at the Fermi level has $\approx 20\%$ character from the axial orbitals (d_{z^2} , $O-p_z$, Cu-4s) within the LDA calculations. The GW reduces this weight down to $\approx 10\%$, but we observe that this remains present for the largest AO displacements. Interestingly, the axial character is nearly suppressed in NCO due to the absence of AO, with d_{z^2} , $O-p_z$ not contributing at all and Cu-4s contributing $\approx 3\%$. This suggests that the physics in NCO is well described by a three band model. We also find that NCO has a significantly reduced $\Delta_x = 0.97$ eV (see Fig. 3) than LCO ($\Delta_x = 1.50$ eV).

We now turn to the optical conductivity (see Fig. 4). We find an optical gap of ≈ 1.8 eV with a sharp onset at

around 2.0 eV, with $\sigma = 920$ (ohm-cm) $^{-1}$, followed by a plateau extending to nearly 3.5 eV, in remarkable agreement with the data extracted from Ref. [17]. This provides a strong validation of the theory for pristine LCO, which is very important: previous theoretical attempts had difficulty in obtaining a good description of the onset and the plateau, and further corrections were invoked. In particular, DMFT calculations of the 6-band model, including the apical oxygen and $d_{z^2-3r^2}$ orbitals, are not able to resolve the discrepancy between theoretical optics and the experiments [18].

This emerges naturally from the QSGW+DMFT. Indeed, the QSGW non-local self energy aligns the O-*p* and the Cu-*d* states very differently than does DFT. There are some discrepancies with experiment: the shoulder and height of the peak are well described, but there are difference in plateau above the shoulder. Also the spectral weight for $\Omega > 6$ eV (not shown) is blue-shifted. Both of these effects are to be expected because of the missing vertex in the RPA [19], a common problem in GW. DMFT corrections are negligible for $\Omega > 3$ eV.

Finally, performing a similar calculation for NCO, we find it to be a correlated metal, with both e_g and t_{2g} orbitals active at the Fermi level. One might expect that its metallic nature would share similarities with the limiting case of large A-O displacements for LCO. We find however that, despite the apparent similarities in the one-particle response functions, the two metallic phases are qualitatively very different, as shown by their two-particle responses. For instance, we find very different magnetic (see Fig. 2e) and charge (see Fig. 2f) susceptibilities. Firstly, the charge fluctuations are peaked at the Γ point, in stark contrast with LCO, where the charge fluctuations are peaked at (π, π) . Second, the background of charge fluctuations in NCO are two orders of magnitude larger than for LCO. Finally, the magnetic susceptibility is peaked at (π, π) , but the peak is relatively narrow, suggesting long-range anti-ferromagnetic super-exchange interactions in direct space.

The spin and charge separation in NCO is strongly observed in the susceptibilities. This suggests that the dynamics can no longer be described in terms of individual particles or single-particle excitations, as pointed out early by P. Anderson [20]. Although it is not a definite proof, our results indicate that NCO is likely to go through a superconducting instability, rather than through a spin- or charge-density wave alone. Our results agree hence with the recent observation that annealed NCO and PCO compounds are superconducting, and not anti-ferromagnetic [4].

We thank Yayu Wang for discussions and sharing insights and experimental data. This work was supported by the Simons Many-Electron Collaboration, and EP-SRC (grants EP/M011631/1 and EP/M011038/1). C.W. gratefully acknowledges the support of NVIDIA Corporation with the donation of the Tesla K40 GPUs used

for this research, and support from the ARCHER UK National Supercomputing Service.

METHOD

We use a recently developed quasi-particle self consistent GW + dynamical mean field theory (QSGW+DMFT) approach to address this problem, as implemented in the Questaal package [10]. Paramagnetic DMFT is combined with nonmagnetic QSGW via local projectors of the Cu 3d states on the Cu augmentation spheres to form the correlated subspace. We carried out the QSGW calculations in the orthorhombic phase of LCO with space group 64/Cmca[15]. DMFT provides a non-perturbative treatment of the local spin fluctuations. We use an exact hybridization expansion solver, namely the continuous time Monte Carlo (CTQMC) [11], to solve the Anderson impurity problem.

The one-body part of QSGW is performed on a $16 \times 16 \times 16$ k-mesh and charge has been converged up to 10^{-6} accuracy, while the (relatively smooth) static self-energy $\Sigma^0(\mathbf{k})$ is constructed on a $4 \times 4 \times 4$ k-mesh from the dynamical GW $\Sigma(\mathbf{k}, \omega)$. $\Sigma^0(\mathbf{k})$ is iterated until convergence (RMS change in $\Sigma^0 < 10^{-5}$ Ry). The DMFT for the dynamical self energy is iterated, and converges in ≈ 10 iterations. The calculations for the single particle response functions are performed with 10^8 QMC steps per core and the statistics is averaged over 64 cores. The two particle Green's functions are sampled over a larger number of cores (192) to improve the statistical error bars. We sample the local two-particle Green's functions with CTQMC for all the correlated orbitals and compute the local polarization bubble to solve the inverse Bethe-Salpeter equation (BSE) for the local irreducible vertex. Finally, we compute the non-local polarization bubble $G(\mathbf{k}, \omega)G(\mathbf{k} - \mathbf{Q}, \omega - \Omega)$ and combined with the local irreducible vertex [12] we obtain the full non-local spin and charge susceptibilities $\chi_{s,c}(\mathbf{Q}, \Omega)$. The susceptibilities are computed on a $16 \times 16 \times 16$ \mathbf{Q} -mesh.

ORBITAL CHARACTER OF BANDS NEAR THE FERMIL LEVEL, PRISTINE CASE

The QSGW bands closest to the Fermi level ($E_F=0$ in Fig. 5), consist of mostly Cu $d_{x^2-y^2}$ (red) with a substantial contribution from O p_x, p_y (blue) orbitals (Table I). Thus near E_F bands are purple. There is also a small but finite contribution from orbitals of axial symmetry (mostly O- p_z but also Cu- d_{3z^2-1} and Cu-4s) on the $A-E_0-T$ and $S-R-Z$ symmetry lines. The Cu-4s weight is most pronounced near the Y point, in a band labelled Cu s . O p_z (orange, below -3 eV) hybridise to some extent with Cu d_{3z^2-1} (green) around -2 eV and the other Cu d orbitals (black, labelled as Cu d), and to

a lesser extent, the bands at E_F .

The LDA bands at the Fermi level consist of strongly mixed Cu- $d_{x^2-y^2}$ (red) and O- p_x, p_y (green) (Fig. 5a) orbitals. The Cu- d_{3z^2-1} orbitals also have strong mixing with primarily apical O- p_z orbital 1.9 eV below the Fermi level. The O- p states are strongly hybridized with most orbital characters throughout the entire window (E_F-8 eV, E_F). However, in contrast to the LDA, QSGW splits out the O- p orbitals from the Cu- d and puts them roughly 2 eV (Fig. 5a) below the (green) band with dominant Cu d_{3z^2-1} character. Also, within QSGW the band character at the Fermi level becomes dominantly Cu- $d_{x^2-y^2}$, with significantly lessened O- p_x, p_y contribution than the LDA.

Finally, the optical absorption predicted by QSGW + paramagnetic DMFT are in good agreement with experiment, as described in the main text.

All the relevant numbers for the contributions from different orbitals to the active band at the Fermi level are shown in the table.

QSGW and LDA compared

When comparing bands of similar color in the first and second columns of Fig. 5, it is evident that there are qualitative similarities but important quantitative differences.

- The x^2-y^2 band is about 50% wider in the LDA, and the asymmetry in the splitting around E_F is inverted.
- Contrary to what would be expected from the wider bandwidth, the density-of-states at E_F is about 50% *larger* in the LDA. This indicates that not only level alignments, but hopping matrix elements are substantially different in the LDA.
- O p (blue and orange) are 1.5-2 eV closer to E_F in the LDA. As a consequence they hybridise much more strongly the Cu d orbitals, in particular the x^2-y^2 and $3z^2-1$ orbitals that drive superconductivity.
- Splitting between Cu x^2-y^2 and $3z^2-1$ orbitals is roughly twice larger in the LDA.
- Orbitals corresponding to those labelled Cu s and La d in the QSGW and LDA panel lie about 1 eV closer to E_F in the LDA. Moreover, Cu s portion to the band labelled ‘‘Cu s ’’ is about half of what it is in QSGW.
- the La f states (dense black, around 3.5 eV in the LDA) should be at around 10 or 12 eV.

It is interesting to note that the non-magnetic bath once coupled with magnetic DMFT, using 82.2 eV for

double counting corresponding to 9 d electrons, does not produce a Mott gap at the Fermi level when LDA is used for the bath, while QSGW+paramagnetic DMFT does. The spectral function computed from DMFT shows the gap opening (Fig. 5a) at the Fermi level within this formalism for the parent LCO, while the DMFT spectral functions (Fig. 5b) when $\delta > 0.045 \text{ \AA}$ has metallic excitations across the Fermi level.

APICAL OXYGEN DISPLACEMENTS AND THE SPECTRAL EVOLUTION

Shifting the apical O has a delicate effect on the QSGW hamiltonian; nevertheless this small change is enough to give rise to dramatic changes when many-body effects are included through DMFT, showing that pristine LCO is in the vicinity of a quantum-critical point.

When O is displaced by $\delta = 0.09 \text{ \AA}$, the Cu d_{3z^2-1} drops about 0.2 eV relative to the x^2-y^2 state, while the O p_z rises by an approximately similar amount. These states come closer together, reflecting the reduction in the hopping matrix element that hybridises them and pushes them apart. At the same time, the O p_{xy} bands rise by $\sim 0.1-0.2$ eV. Fig. 5 shows valence bands resolved on a fine energy scale for $\delta = 0$ and $\delta = 0.09 \text{ \AA}$, where the shifts can be seen in detail. As a secondary effect, the Cu x^2-y^2 bandwidth is slightly reduced.

The lowest bands above E_F are primarily of La character, especially La d . La does not hybridize strongly with the Cu and O, but there is a significant evolution in charge transfer to it with δ . The shift in the bands is a consequence mainly of the difference in electrostatic potentials at the La and Cu nuclei. In the $\delta = 0.09 \text{ \AA}$ structure this difference is ~ 1.5 eV larger than in the pristine compound.

-
- * swagata.acharya@kcl.ac.uk
- [1] N.P. Armitage, D. H. Lu, C. Kim et al., Phys. Rev. B. **68**, 064517 (2003).
 - [2] Y. Tokura, A. Fujimori, H. Matsubara et al. Phys. Rev. B **39**, 9704 (1989).
 - [3] H. Takagi, S. Uchida, and Y. Tokura, Phys. Rev. Lett. **62**, 1197 (1989).
 - [4] M. Horio, T. Adachi, Y. Mori et al., Nat. Comm. **7**, 10567 (2016).
 - [5] P. Cai, W. Ruan, Y. Peng et al., Nature Physics **12**, 1047-1051 (2016).
 - [6] E. Pavarini, I. Dasgupta, T. Saha-Dasgupta et al., Phys. Rev. Lett. **87**, 047003 (2001).
 - [7] C. Weber, C. Yee, K. Haule et al., Eur. Phys. Lett. **100**, 37001 (2012).
 - [8] A. Georges, G. Kotliar, W. Krauth et al., Rev. Mod. Phys., **68**, 0034 (1996).
 - [9] K. Held, O. K. Andersen, M. Feldbacher et al., J. Phys.: Condens. Matter, **20**, 064202 (2008).
 - [10] The Questaal code is freely available at <http://www.questaal.org>. Our GW implementation was adapted from the original ecalj package, now at <https://github.com/tkotani/ecalj/>.
 - [11] K. Haule and G. Kotliar, Phys. Rev. B **76**, 104509 (2007).
 - [12] H Park, K. Haule, and G. Kotliar, Phys Rev Lett. **107**, 137007 (2011).
 - [13] A.-M. Dare, L. Chen, and A.-M. S. Tremblay et al., Phys. Rev. B **49**, 4106 (1994).
 - [14] L. Fratino, P. Smon, G. Sordi et al., Sci. Rep. **6**, 22715 (2016).
 - [15] M. Reehuis, C. Ulrich, K. Proke et al., Phys. Rev. B **73**, 144513 (2006).
 - [16] J. Zaanen, G. A. Sawatzky, and J. W. Allen, Phys. Rev. Lett. **55**, 418 (1985).
 - [17] S. Uchida, T. Ido, H. Takagi et al., Phys. Rev. B, **43** 7942 (1991).
 - [18] X. Wang, H. T. Dang, and A. J. Millis Phys. Rev. B **84**, 014530 (2011).
 - [19] S. Albrecht, L. Reining, R. Del Sole, et al., Phys. Rev. Lett. **80**, 4510 (1998).
 - [20] P. Anderson, Physica C: Superconductivity **341**, 9 (2001).

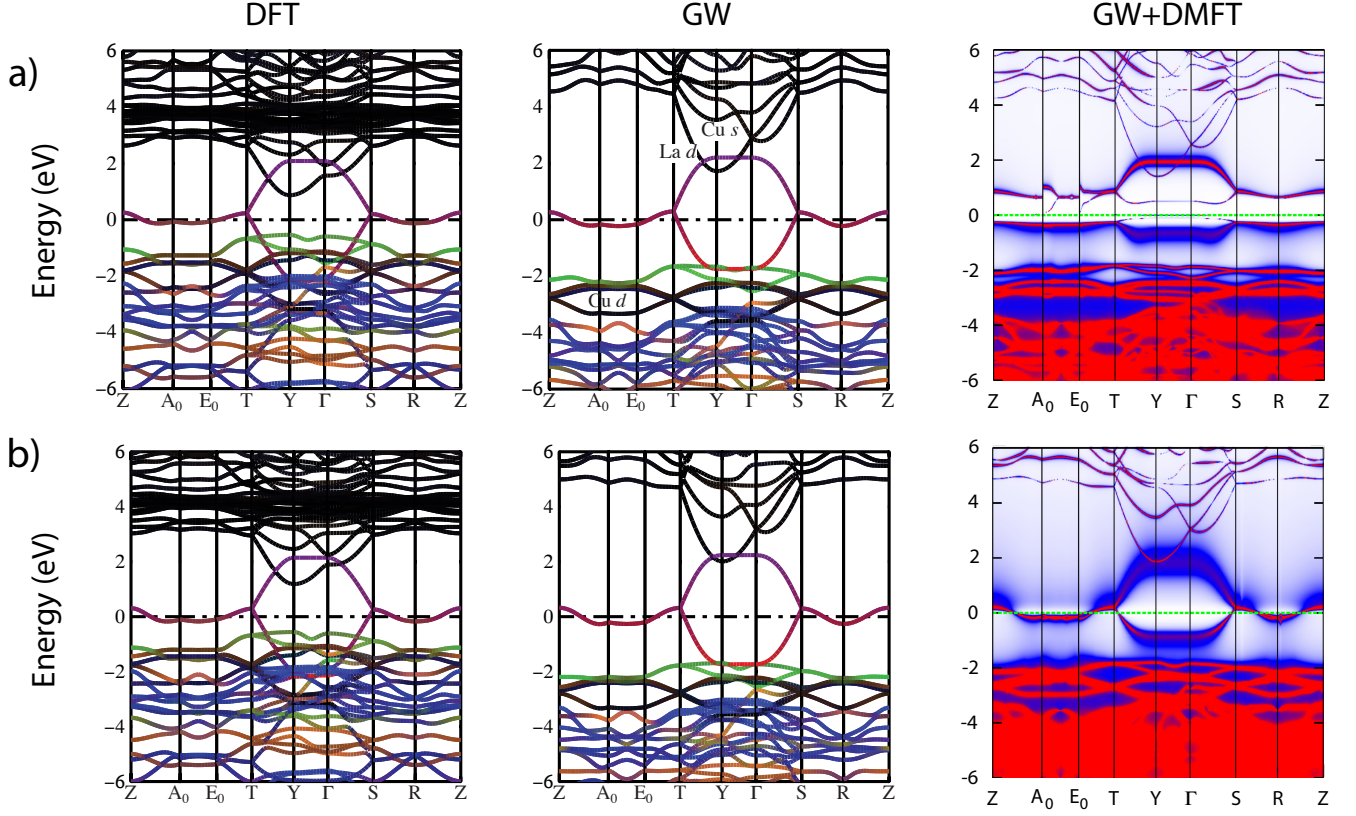


FIG. 5. **Band structure:** Comparison of the band structure as obtained from DFT, QSGW, and QSGW+DMFT. a) pristine LCO ($\delta=0$). b) compound with apical oxygens displaced by $\delta=0.09$ Å. c) zoomed in band structure for pristine LCO and d) for distorted LCO $\delta=0.09$ Å. Colors reflect the orbital character of the bands as follows: Cu $d_{x^2-y^2}$ (red); Cu d_{3z^2-1} (green), near -2 eV in QSGW; O- p_{xy} (blue), between -3 eV and -5 eV in QSGW; O- p_z (orange), between -3 eV and -5 eV in QSGW. The band near 3.3 eV at Y has significant Cu s character, and it also admixes into the Cu $d_{x^2-y^2}$ near E_F .

Table									
Compound	Z	Γ	N_{eff}	Δ_x in eV	T_c^{max} in K	Δ in eV	Cu $d_{x^2-y^2}$	Axial orbitals	O- p_{xy}
LCO ($\delta = 0$) QSGW	0.00	11.4	0.3	-1.53	34	0.78	0.5437	0.108	0.2630
LCO ($\delta = 0.03$) QSGW	0.02	0.41	3.4	-1.49	79	1.0	0.5454	0.105	0.2615
LCO ($\delta = 0.05$) QSGW	0.08	10^{-4}	42.6	-1.45	53	0	0.5471	0.092	0.2607
LCO ($\delta = 0.09$) QSGW	0.41	10^{-9}	86.0	-1.37	11	0	0.5507	0.086	0.2591
LCO ($\delta = 0$) LDA							0.40067	0.22	0.2798
NCO QSGW	0.44	10^{-6}	98.3	-0.97	25	0	0.63007	0.033	0.2520

TABLE I. Quasi-particle weight Z, Imaginary part of the self energy extrapolated to zero frequency $\Gamma = -\Sigma''(i\omega \rightarrow 0)$, optical mass N_{eff} (optical conductivity integrated up to 2.3 eV), charge transfer energy Δ_x , d-wave superconducting transition temperature T_c^{max} , single particle charge gap Δ , relative weights of the Cu $d_{x^2-y^2}$, axial orbitals (Cu d_{z^2} , O- p_z , Cu $4s$) and O- p_{xy} to the active band at the Fermi level. We perform calculations for all relevant compounds within QSGW+DMFT (marked as QSGW in the table against respective compounds). We show the LDA results only for LCO as a comparison against the QSGW results. Z, Γ , N_{eff} , T_c^{max} and Δ are extracted by post-processing the results from fully converged QSGW+DMFT.